Cerebral Cortex April 2013;23:859–872
doi:10.1093/cercor/bhs080
Advance Access publication March 27, 2012

Bilateral Subcortical Heterotopia with Partial Callosal Agenesis in a Mouse Mutant

G. D. Rosen[1], N. G. Azoulay[1], E. G. Griffin[1], A. Newbury[1], L. Koganti[1], N. Fujisaki[2,3], E. Takahashi[2,3,4,5], P. E. Grant[2,3,4,5,6], D. T. Truong[7], R. H. Fitch[7], L. Lu[8] and R. W. Williams[8]

[1]Department of Neurology, Beth Israel Deaconess Medical Center, Boston, MA 02215, USA, [2]Department of Radiology, Harvard Medical School, Charlestown, MA 02129, USA, [3]A. A. Martinos Center for Biomedical Imaging, Massachusetts General Hospital, Charlestown, MA 02129, USA, [4]Division of Newborn Medicine, Department of Medicine, Children's Hospital Boston, Harvard Medical School, Boston, MA 02115, USA, [5]Fetal-Neonatal Neuroimaging and Developmental Science Center, Children's Hospital Boston, MA 02115, USA, [6]Department of Radiology, Children's Hospital Boston, Boston, MA, Harvard Medical School, Boston, MA 02115, USA, [7]Department of Psychology, University of Connecticut, Storrs, CT 06269, USA and [8]Department of Anatomy and Neurobiology, Center for Integrative and Translational Genomics, University of Tennessee Health Science Center, Memphis, TN 38163, USA

Address correspondence to Glenn D. Rosen, Department of Neurology, E/CLS-643, Beth Israel Deaconess Medical Center, 330 Brookline Avenue, Boston, MA 02215, USA. Email: grosen@bidmc.harvard.edu.

Cognition and behavior depend on the precise placement and interconnection of complex ensembles of neurons in cerebral cortex. Mutations that disrupt migration of immature neurons from the ventricular zone to the cortical plate have provided major insight into mechanisms of brain development and disease. We have discovered a new and highly penetrant spontaneous mutation that leads to large nodular bilateral subcortical heterotopias with partial callosal agenesis. The mutant phenotype was first detected in a colony of fully inbred BXD29 mice already known to harbor a mutation in *Tlr4*. Neurons confined to the heterotopias are mainly born in midgestation to late gestation and would normally have migrated into layers 2–4 of overlying neocortex. Callosal cross-sectional area and fiber number are reduced up to 50% compared with coisogenic wildtype BXD29 substrain controls. Mutants have a pronounced and highly selective defect in rapid auditory processing. The segregation pattern of the mutant phenotype is most consistent with a two-locus autosomal recessive model, and selective genotyping definitively rules out the *Tlr4* mutation as a cause. The discovery of a novel mutation with strong pleiotropic anatomical and behavioral effects provides an important new resource for dissecting molecular mechanisms and functional consequences of errors of neuronal migration.

Keywords: diffusion spectrum imaging, neuronal migration, rapid auditory discrimination, recombinant inbred, stereology

Introduction

Mutations and environmental perturbations that disrupt migration of neurons and patterns of connectivity have been linked to a range of neurological and psychiatric disorders (Kuzniecky 2006; Leventer et al. 2008; Andrade 2009). These disorders include subcortical band heterotopia (des Portes et al. 1998; Gleeson et al. 1998), periventricular nodular heterotopias (Dobyns et al. 1997; Pilz et al. 1998; Ferland et al. 2009), cobblestone lissencephaly (Dobyns et al. 1996), classical lissencephaly (Gleeson 2000; Lammens 2000; Leventer et al. 2000), and polymicrogyria (Chang et al. 2004; Guerrini and Filippi 2005; Jansen and Andermann 2005). Mutant alleles underlying some of these malformations were first identified in mouse models nearly 40 years ago (Caviness et al. 1972) and many have now been linked to developmental disorders in humans, including *LIS1*, *DCX*, *TUBA1A*, *ARX*, *RELN*, *POMT1*, *POMT2*, *FKTN*, *FKRP*, and *LARGE* (for review, see Verrotti et al. 2010).

Gene knockouts and mutations in rodent models have provided superb tools to explore mechanisms of neocortical assembly. Small molecular layer ectopias have been described in a variety of inbred mouse strains (Sherman et al. 1987, 1990; Ramos et al. 2008), and larger subcortical band heterotopias have been reported in mice (Croquelois et al. 2009) and rats (Lee et al. 1997; Chen et al. 2000; Trotter et al. 2006), although the specific genes and sequence variants responsible for these malformations have not yet been defined. A variety of knockout mice have been generated that disrupt neuronal migration (Bilasy et al. 2009; Soumiya et al. 2009; Goryunov et al. 2010), but most lines are perinatally lethal and therefore not useful to study functional effects at maturity.

As part of larger project involving the dissection of molecular and genetic networks modulating neuronal migration, we screened brains from 8 to 14 animals from each of 72 genetically defined and fully inbred strains that are part of the BXD strain family. We serendipitously discovered that 2 of 10 brains from the BXD29/TyJ strain had bilateral nodular subcortical heterotopias in the caudal/medial neocortex accompanied by partial callosal agenesis. All eight unaffected BXD29/TyJ cases were born prior to 1998, whereas those cases with the bilateral malformations were born in 2004. Coincidently, a spontaneous mutation was reported in this strain in 2004 (Cook et al. 2004). These authors discovered that the BXD29/TyJ strain was completely insensitive to inhalation of the bacterial endotoxin, lipopolysaccharide (LPS). Subsequent investigation showed that the mutation was caused by an 8 bp insertion in the *Toll-like receptor 4* gene (*Tlr4*) (Cook et al. 2006). The original BXD29/TyJ strain was re-derived from 1979 frozen stock and assigned the initial designation of BXD29/Ty, whereas the original line, now with the mutation in *Tlr4,* was redesignated BXD29-*Tlr4*$^{lps\text{-}2J}$/J. In this experiment, we have studied genetic, developmental, anatomical, and behavioral differences between the BXD29-*Tlr4*$^{lps\text{-}2J}$/J line and the rederived BXD29/Ty wildtype strain. We report here that the malformation is 100% penetrant, appearing bilaterally in all animals in the BXD29-*Tlr4*$^{lps\text{-}2J}$/J strain. The subcortical heterotopia is invariant in its location and is comprised primarily of neurons destined for layers 2–4 of the neocortex. There is a 50% reduction in the midsagittal area of the corpus callosum (MSACC), and diffusion spectrum imaging confirms a decrease in the number of callosal and cingulum fibers. Mutant mice have a remarkable and selective

defect in rapid auditory processing. Backcross experiments and genotyping demonstrate that the malformation is unlinked to the *Tlr4* mutation.

Materials and Methods

Subjects

All procedures were approved by the Institutional Animal Care and Use Committee of Beth Israel Deaconess Medical Center and the University of Connecticut. For these experiments, we used BXD29-*Tlr4*$^{lps\text{-}2J}$/J (JAX stock number 000029, here referred to as mutant) and BXD29/Ty (JAX stock number 010981, here referred to as wildtype) mice that were originally obtained from the Jackson Laboratory (Bar Harbor, ME, USA). These 2 substrains are a coisogenic pair currently confirmed to differ only at the *Tlr4* locus. In addition, we obtained 2 strains of mice on a C57 background known to have *Tlr4* mutations (B6.B10ScN-*Tlr4*$^{lps\text{-}del}$/JthJ and C57BL/10ScNJ) from the Jackson Laboratory ($N = 6$ for each strain) and *Tlr2*–/– and *Myd88*–/– null mutant mice courtesy of Dr Jacob Sloane (for each strain, $N = 4$).

Histology

Mice were either deeply anesthetized (combination of Xylazine and Ketamine 100 mg/mL and 60 mg/kg, respectively) sacrificed by transcardial perfusion with 0.9% saline followed by 4% paraformaldehyde (older than postnatal day 5, P5), or decapitated and immersion fixed (younger than P3). A subset of brains were embedded in celloidin following postfixation for at least 1 week, where the brains were dehydrated in graded ethanols and embedded in 12% celloidin. They were then cut in the coronal, sagittal, or horizontal plane at 30 μm, stained with cresyl violet, and every 10th section was mounted on glass slides with Permount. The remaining animals were prepared for processing by freezing microtome (≥P5) or cryostat (≤P3). The brains were removed from the skull and postfixed for 24 h before being cryoprotected in 10% and then 30% sucrose phosphate buffer. The brains were sectioned coronally at either 40 μm on a freezing microtome or at 14 μm on a cryostat. One series of every tenth section was stained for Nissl substance using thionin. Adjacent series of free-floating frozen sections were processed for immunohistochemistry as detailed below.

Immunohistochemistry

Adjacent series of sections from P21 and older brains were processed for immunohistochemical detection of transcription factors that have relatively specific laminar distribution patterns in the cortex. These included CUX1 (CDP, M 222, Santa Cruz Biotechnology, Santa Cruz, CA, 1:1000), FOXP2 (N 16, Santa Cruz Biotechnology, 1:200), connective tissue growth factor (CTGF, L 20, Santa Cruz Biotechnology, 1:50). Expression of *Cux1* message and CUX1 protein is restricted to neurons in layers 2–4 (Nieto et al. 2004); FOXP2 antibodies labels neurons in layers 5 and 6 of the cortex (Keays et al. 2007); and CTGF is a highly selective marker of layer 6b neurons (Heuer et al. 2003). 5-bromo-2′-deoxyuridine (BrdU) positive neurons were labeled with anti-BrdU antibodies (BD Biosciences, San Jose, CA, 1:1000), and myelinated fibers were detected with antibodies against myelin basic protein (MBP, C-16, Santa Cruz Biotechnology, 1:10 000). Immunoperoxidase activity was detected using 3,3-diaminobenzidine (DAB; Vector Labs) according to ABC protocols. Immunohistochemistry of celloidin-embedded sections proceeded identically but only after removal of celloidin by 2 washes in 1:1 solution of ether and 100% ethanol and subsequent rehydration. The tissue was mounted and coverslipped with Permount mounting medium (Fisher Scientific, Waltham, MA).

BrdU

Pregnant mice carrying embryonic (E) days E12.5, E14.5, and E16.5 fetuses were anesthetized with isoflurane (5%) and intraperitoneally injected with 50 mg/kg of BrdU (Sigma Aldrich, St. Louis, MO, 10 mg/mL solution). Their pups were killed at P21, their brains removed, and processed via frozen sectioning on a sliding microtome.

Stereology

Stereological estimations of cortical, cerebellar, hippocampal, striatal, total brain, and heterotopia volume were performed using Stereo Investigator (MBF Biosciences, Williston, VT) using point counting and Cavalieri's rule (Gundersen and Jensen 1987; Rosen and Harry 1990). MSACC was estimated by measuring the linear dorsal–ventral distance at the midline of the corpus callosum in systematic serial sections and using Cavalieri's rule to compute the area. Estimation of the number of neurons in the heterotopia was performed using the optical fractionator probe. The number of neurons in layers 2–4 in the area overlying the heterotopia in mutant mice was estimated using the optical fractionator and compared with the number of layer 2–4 neurons in homologous regions of the matched wildtype mice. Analysis of variance (ANOVA) procedures were used to determine statistical significance.

High–Angular Resolution Diffusion Imaging

Four BXD29-*Tlr4*$^{lps\text{-}2J}$/J mutant and 4 BXD29/Ty wildtype mice were perfused as described above. Fixed brains were transferred to the Martinos Center for Biomedical Imaging (MCBI), where they were fixed for an additional week in 4% paraformaldehyde solution containing 1 mM gadolinium (Gd-DTPA) magnetic resonance imaging contrast agent to reduce the T_1 relaxation time while ensuring that enough T_2-weighted signal remained. For image acquisition, the brains were placed in Fomblin. Imaging was conducted blindly with respect to substrain.

Scanning Parameters

Brains were scanned on a 4.7 T Bruker Biospec MR system. The pulse sequence used for image acquisition was a 3D diffusion-weighted spin-echo echo-planar imaging sequence, time repetition (TR)/time echo (TE) 1200/45.47 ms, with an imaging matrix of 70 × 70 × 80 pixels. Spatial resolution was 250 × 250 × 250 μm. Sixty diffusion-weighted measurements ($b = 4000$ s/mm^2) and one non–diffusion-weighted ($b = 0$) measurement were acquired, with small delta = 12.0 ms, large delta = 24.2 ms. The total acquisition time was approximately 2 h for each imaging session.

Diffusion Data Analyses—Tractography

We reconstructed orientation distribution function in each voxel using HARDI method and reconstructed tractography pathways using a streamline algorithm for diffusion tractography (Mori et al. 1999). The same approach was used in previous publications (Schmahmann et al. 2007; Wedeen et al. 2008; Takahashi et al. 2011). Trajectories were propagated by consistently pursuing the orientation vector of least curvature. Diffusion Toolkit and TrackVis (http://trackvis.org) were used to reconstruct and visualize pathways. The color coding of tractography pathways is based on a standard RGB code, applied to the vector between the endpoints of each fiber.

We terminated tracking when the angle between 2 consecutive orientation vectors was greater than the given threshold (40°) for each specimen. As in previous studies, no fractional anisotropy (FA) threshold was applied (Schmahmann et al. 2007; Wedeen et al. 2008, Takahashi et al. 2010, 2011; Vishwas et al. 2010). In many tractography studies, FA values are used to terminate fibers in the gray matter, which in adults has lower FA values than the white matter. However, as one of the objectives of our study was to detect fibers in abnormal brain areas that possibly have low FA values, we used brain mask volumes to terminate tractography fibers instead of the FA threshold. This method has been used previously (Takahashi et al. 2010, 2011) and is an acceptable alternative (Schmahmann et al. 2007; Wedeen et al. 2008).

Callosal connections were isolated as fibers passing through the manually drawn region of interest (ROI) that included the entire corpus callosum in the midline, ensuring that other fiber pathways were not contributing. Corticospinal tracts were isolated by placing ROIs in the spinal cord and also in the cerebrum, selecting fibers passing through both ROIs. Setting a length threshold between 0 and 6 mm and excluding pathways that crossed the midline also identified intrahemispheric pathways. Placing 2 ROIs in the cingulate gyrus isolated the cingulum tracts. Identification of pathways was verified by

3 tractographers with experience in rodents, including a neuroradiologist (P.E.G.).

FA and apparent diffusion coefficient (ADC) values were calculated by fitting the data to the usual tensor model. FA and ADC values on each identified pathway (callosal, corticospinal, etc.) are automatically derived by TrackVis once we identify the pathways.

Behavior

Behavioral tasks were chosen with the intent to assess processing domains that have previously revealed deficits in models of cortical migrational disruption (Fitch et al. 1994, 2008; Clark et al. 2000; Peiffer et al. 2004). Additional tasks, such as the rotorod, hippocampally dependent Morris water maze, and nonhippocampal nonspatial water maze, were selected to assess: 1) whether deficits might be seen on tasks associated with structures where no visible disruptions are seen in this model (suggesting global and pervasive reorganizational effects on many neural systems) or 2) whether a pattern of deficits on specific tasks and not others might illuminate more specific processing domains impacted by this genetic anomaly.

Subjects

Eight male BXD29/Ty wildtype and eight matched BXD29-*Tlr4*$^{lps\text{-}2J}$/J mutants were obtained from the Jackson Laboratory and housed singly in standard lab cages (12 h light/dark cycle) with food and water ad lib. Mice were tested at maturity (P188–P242) on all behavioral paradigms. Following behavioral testing, mice were weighed, anesthetized using a mix of Ketamine and Xylazine (100 and 15 mg/kg, respectively), and perfused transcardially with 0.9% saline followed by 4% paraformaldehyde. Brains were postfixed in 4% paraformaldehyde.

Startle Reduction Paradigm

The startle reduction paradigm utilizes a startle-eliciting stimulus (SES; 105 dB, 50 ms white noise burst) to produce an acoustic startle reflex (ASR)—a large-amplitude involuntary response to the SES. When a prepulse prior to an SES is detected by the mouse, the ASR response should attenuate (prepulse inhibition). However, when a prepulse does not precede an SES, the SES should evoke a greater ASR response in comparison to a cued SES. Attenuation of the startle response is quantified as a percent of cued to uncued trials. Subjects were placed on individual load-cell platforms as described previously (Fitch et al. 2008). Auditory stimuli were produced using a computer with custom programmed software and a Tucker Davis Technologies (Alachua, FL) real-time processor (RP2). Sound files were created and played using a custom program (RPvdsEx), amplified using a Niles SI-1260 Systems Integration Amplifier (Niles Audio Corporation, Carlsbad, CA), and delivered via powered speakers located ~53 cm above each platform.

Normal single tone. The normal single tone task provided a baseline measure for each subject that revealed whether the subject had 1) hearing deficits and 2) impaired startle gaiting behaviors that would exclude the subject from further auditory testing. The testing session comprised of 104 cued/uncued trials presented pseudorandomly with variable intertrial intervals (ITI) ranging from 16 to 22 s in length. Uncued trials were a silent background with an SES. Cued trials presented a 50-ms 75-dB 2300-Hz tone pip, 100 ms prior to the SES. Normal single tone testing occurred on days P185 and P199 and on days P247 and P261. All mice were able to detect the prepulse and attenuate their startle response, thus all mice were used for further auditory testing.

Silent gap. The task comprised of variable duration silent gaps (cue) embedded within continuous broadband presented 100 ms prior to the presentation of the SES. During an uncued trial, the silent gap was 0 ms in duration (no gap condition). ITIs were pseudorandomly varied, ranging from 16 to 24 s throughout the 300-trial session. Two different variations of the silent gap test were used—long-gap duration and short-gap duration—both of which occurred over 5 days of testing. For the long-gap task, trials were comprised of silent gap cues ranging from 50 to 300 ms in length, and the short gap task comprised of silent gap cues ranging from 2 to 100 ms in duration.

Motor Assessment

Sensorimotor ability and balance were measured using a rotarod test. For this task, subjects were placed on a rotating cylindrical drum that gradually accelerated from 4 to 40 rpm over a span of 2 min. Mice were given 4 consecutive trials, and the length of time on the rotating drum without falling was recorded and averaged across the 4 trials for further statistical analysis.

Water Maze Assessment

All mice were tested in a water escape task as a control procedure to ensure that subjects did not have underlying motivational, motor, or visual impairments that may potentially prevent effective performance on the subsequent series of water maze tests. Mice were placed into one end of a tub (103 cm × 55.5 cm) filled with room temperature water (21°C), where they were required to swim to a visual platform (8.5 cm in diameter) located at the opposite end. Latency to the visible platform was recorded. All subjects effectively performed the task, showing no effect of Strain in the latency to platform.

Morris water maze. The Morris water maze (MWM) was used to assess the subjects' spatial learning and memory ability over a period of 5 testing days. The goal of the MWM was to locate a submerged invisible platform (8.5 cm in diameter), 2 cm below the surface of the water. For the duration of MWM testing, the hidden platform remained in a fixed location (southeast quadrant) within a round black tub (122 cm in diameter) surrounded by static, salient, extra maze cues (painted shapes on wall, location of experimenter, door, etc.). A test day consisted of 4 trials (separated by approximately 5 min) with the subjects' starting location randomized to a different compass point (north, south, east, and west) for each trial. Subjects were allowed a maximum of 45 s per trial to find the submerged platform. On day 1 of MWM testing (prior to first trial) subjects were placed on the submerged platform for 10 s, removed from the platform, and then replaced back into the water at one of the compass locations. Latency to reach the platform was measured using a stopwatch and recorded for all trials, subjects, and days. The total sum of latencies to reach the target platform during all 4 trials was calculated for each individual subject on each individual testing day and used for further statistical analysis.

Nonspatial water maze. As in the MWM, the goal of the nonspatial water maze (NSWM) was to also locate a submerged hidden platform within a round tub (same dimensions as MWM) filled with room temperature water. However, unlike the MWM, the round tub now contained a black rotating insert with saliently painted intramaze cues (vertical black and white stripes, horizontal black and white stripes, black polka dots on a white background, and white polka dots on a black background). For this task, the location of the submerged platform was always associated with one of the intramaze cues (vertical black and white stripe). Thus, for this task, the subjects had to rely on local cues to find the hidden platform while placed into the pool at a fixed starting location (north). A test day consisted of 4 trials with the location of the platform (and associated intramaze cue) pseudorandomly rotated into a different quadrant (southwest, southeast, northwest, and northeast) of the pool for each individual trial. Subjects were given a maximum of 45 s per trial to locate the platform. On day 1 of NSWM testing (prior to the first trial) subjects were placed on the submerged platform for 10 s, removed from the platform, and replaced into the water at the north compass point. Latency to reach the platform was measured using a stopwatch and recorded for all trials, subjects, and days. The total sum of latencies to reach the target platform was calculated for each individual subject on each individual day of testing and used for further statistical analysis.

Genetics

Backcross Experiment

The pattern of inheritance of the mutation was determined by crossing wildtype females to mutant males to create coisogenic F1 progeny (BXD29/TyJ × BXD29/*Tlr4*$^{lps\text{-}2J}$/J). These F1 progeny segregate for

the previously known variant *Tlr4* and possible novel mutations that contribute to the heterotopia. F1 progeny of both sexes were backcrossed to the mutant stock. A set of 51 of these backcross progeny were phenotyped. If the mutation causing heterotopia were a fully penetrant recessive allele then none of the F1 progeny and approximately half of the backcrossed progeny would be mutants. Deviations from expectation toward lower proportions of mutants in the backcross would indicate lower penetrance and potential multigenic control.

Genomic DNA from the 51 backcross progeny was extracted from spleen using the HotSHOT method (Truett et al. 2000). Two pairs of nested primers were designed to genotype the *Tlr4* mutant allele. The first pair corresponds to a region in exon 3 immediately upstream of the insertion and immediately 3′ of an *EcoRI* restriction site (5′-ACATTCCTGTAAGTTACCTGCATATTT-3′ and 5′-GCTAAACGTTGGAGAAAGCACA-3′, respectively). The second pair flanks the 8-nucleotide repeat (TCTTTCTT) in exon 3 (5′-GCTTCCCTATTGGACAGCTT-3′ and 5′- CCTGAAAGGCTTGGTCTTGA-3′). Target DNA was amplified using Roche FastStart PCR reagents (1 × PCR buffer, 1.92 mM $MgCl_2$, 0.25 units of *Taq* DNA polymerase, 0.2 mM of each deoxynucleotide, and 10 nM of the primers) with 50 ng of DNA. A standard PCR protocol was used for both rounds of amplification (95 °C for 4 min, 35 cycles up to 95 °C for 30 s, 55 °C for 30 s, and 72 °C for 1 min) and 72 °C for 7 min for the final extension. Following the first PCR reaction, an aliquot of the amplicon was used as template for a reaction. The final product was run on an agarose gel. Only the wildtype BXD29/TyJ generates a single band at molecular size 230 bp.

Image Processing

Photomicrographs were adjusted for exposure and sharpened (unsharp mask filter) using Adobe Photoshop CS5 (Adobe Inc., San Jose, CA). Some brightfield images were acquired using the Virtual Slice Module of Neurolucida. Image montages were created in Adobe Illustrator (Adobe Inc.).

Results

BXD29 Mutant Mice Have Midline Bilateral Nodular Heterotopias and Partial Agenesis of the Corpus Callosum

In the initial screen, we examined 2 BXD29-*Tlr4*$^{lps\text{-}2J}$/J mutant and 8 BXD29/Ty cases in The Mouse Brain Library (www.mbl.org) and found that none of the wildtype BXD29/Ty mice had any evidence of malformations, whereas both BXD29-*Tlr4*$^{lps\text{-}2J}$/J mice exhibited bilateral nodular subcortical heterotopias with partial callosal agenesis. In order to assess the frequency of malformations, we screened 17 mutant and 16 wildtype mice obtained directly from the Jackson Laboratory (Bar Harbor, ME, USA) colony (8 mutants and 8 wildtypes were behaviorally tested and subsequently stereologically analyzed) and confirmed that the malformations were seen in all mice from the mutant substrain, that is, the phenotype was 100% penetrant. The nodular heterotopias are always located at the border between retrosplenial cortex and somatosensory or visual cortical regions and are bilateral. Myelinated fibers surround and traverse the heterotopia (Fig. 1). Heterotopias comprise approximately 1.5–3% of the neocortical volume and contain 144 000 ± 13 600 neurons.

To test whether the mutant phenotype has more global and quantitative effects on brain morphology, we measured the volume of cerebellum, hippocampus, striatum, neocortex, as well as total brain volume across 8 wildtype and 8 mutant brains. Surprisingly, volumes of regions were modestly but nonsignificantly larger (3–6%) in all 4 regions of the mutants (Table 1). However, total brain volume was significantly greater in mutants by ~10% ($F_{1,13}$ = 13.8, P < 0.01), suggesting that the mutation does have broader developmental effects.

In addition to the bilateral nodular heterotopias, each mutant also exhibited partial agenesis of the corpus callosum (Fig. 2). The rostral portion of the callosum appears normal, but more caudal levels of the callosum corresponding to the heterotopia itself are disrupted. The corpus callosum in mutants is significantly smaller than that of the wildtype—approximately a 50% reduction in midsagittal area ($F_{1,14}$ = 67.1, P < 001; Table 1).

Is the heterotopia due to the known *Tlr4* mutation? We examined brains from 2 lines of mice—C57BL/10ScNJ and B6.B10ScN-*Tlr4*$^{lps\text{-}del}$/J. Both lines carry the *Tlr4*$^{lps\text{-}del}$ allele and are insensitive to LPS stimulation. In addition, we screened strains where genes related to the *Tlr4* pathway were knocked out—one with a targeted mutation of *Tlr2* (B6.129-*Tlr2*^{tm1Kir}/J) and the other with a targeted mutation to *MyD88*. None of these mice had any evidence of neocortical malformation or partial agenesis of the corpus callosum. These results suggest that the known *Tlr4* mutation is not modulating the forebrain phenotype in the mutant.

The Heterotopia Is Subcortical and Is Comprised of Neurons Generated in Midgestation to Late Gestation

We examined the pattern of CUX1 immunoreactivity in mutant and wildtype mice (Fig. 3). In mutants, there were large numbers of CUX1+ neurons contained within the nodular heterotopia. At the border of the heterotopia, there were CUX1+ neurons in layer 5 (Fig. 3*A*). In contrast, the distribution of CUX1+ neurons in the cerebral cortex was identical to that previously reported (Nieto et al. 2004), with CUX1+ neurons located exclusively in layers 2–4 in the medial cortex (Fig. 3*B*), and little or no immunoreactivity in the subgranular layers. There was a diminution of CUX1+ neurons in layers 2–4 directly superior to the heterotopia when compared with wildtype. We then estimated the number of Nissl-stained neurons in layers 2–4 in the cortex directly overlying the heterotopia in mutant and in the homologous region of matched wildtype mice. Repeated measures ANOVA found that there was a significant 20% decrease in neurons in the mutant mice as compared with wildtype ($F_{1,7}$ = 7.2, P < 0.05; 130 593 ± 13 792 vs. 163 984 ± 18 394, respectively). These results suggest that neurons normally destined for layers 2–4 of the cerebral cortex fail to migrate to their expected location and are positioned within the malformation.

FOXP2 is expressed in layer 5 and 6 neurons in the neocortex (Ferland et al. 2003; Hisaoka et al. 2010). This pattern of expression was seen in both the mutant and wildtype (Fig. 3*C,D*). In the case of the mutant, FOXP2+ neurons were seen directly superior to the nodular heterotopia and only occasionally in the heterotopia. CTGF immunoreactive neurons were found in layer 6b in the cerebral cortex (Heuer et al. 2003). Both mutant and wildtype strains exhibited this same pattern. In the case of the mutant, CTGF+ neurons were located superior to the nodular heterotopia, and there were no CTGF+ neurons in the heterotopia itself (Fig. 3*E,F*). Taken together, the position of laminar markers suggests that these heterotopias are 1) subcortical, and 2) are comprised predominantly of neurons normally destined to the upper laminae of the cerebral cortex.

We obtained mutant and wildtype mice from our breeding colony at embryonic age (E) 17, P1, P3, P5, P7, P10, and P14 and tracked the progression of the midline heterotopias. There was no direct evidence of heterotopia formation in the E17 mutant (Fig. 4*A*). By P1 (Fig. 4*B*), dense collections of heterotopic neurons are visible at the midline, and their density does not

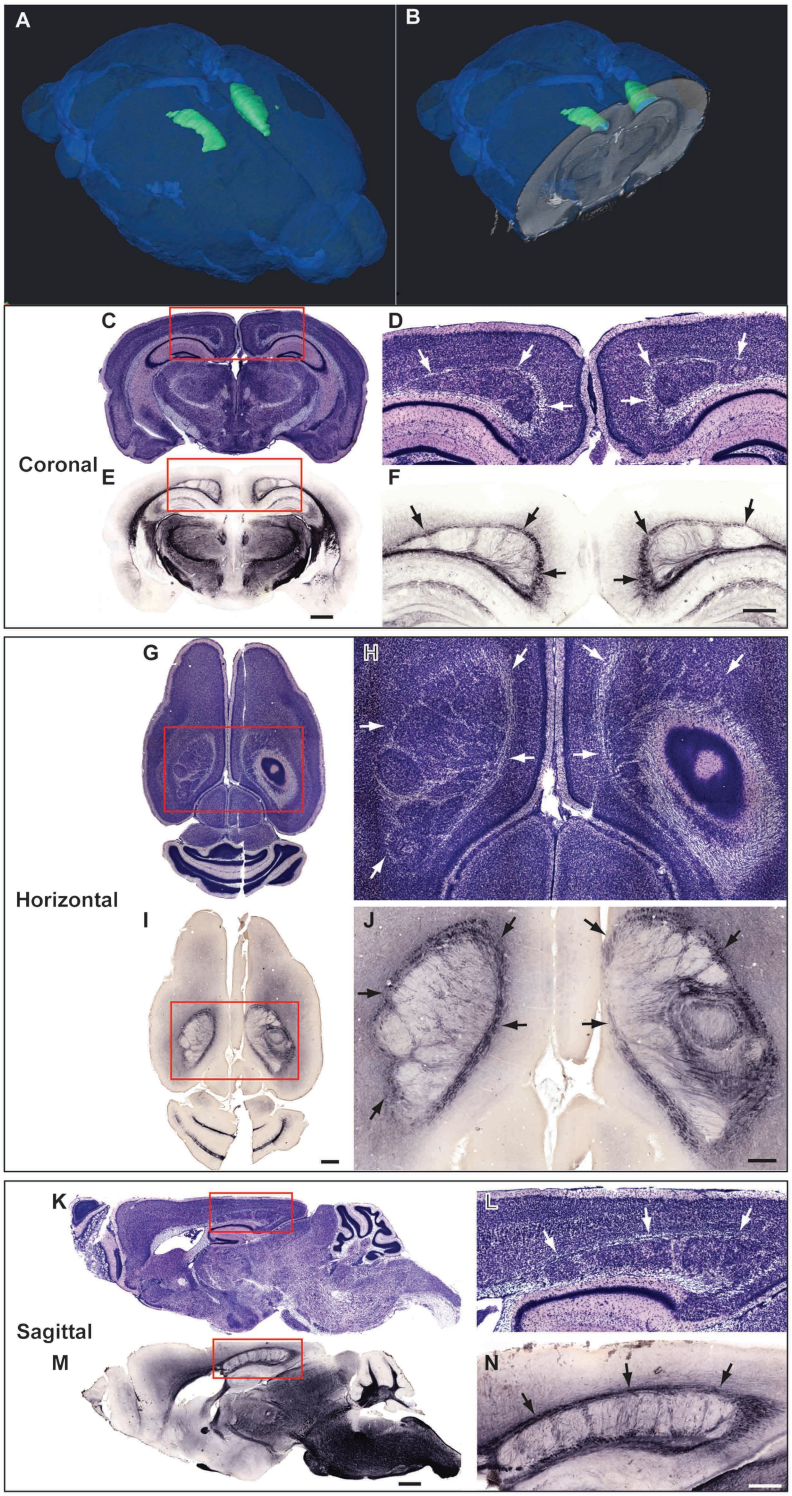

Figure 1. Bilateral midline neocortical nodular heterotopias in BXD29-*Tlr4*$^{lps\text{-}2J}$/J mutant mouse neocortex. (*A*,*B*) 3D reconstruction of bilateral midline nodular heterotopia reconstructed from high-resolution magnetic resonance imaging (courtesy of G.A. Johnson, Duke Center for In Vivo Microscopy). (*C*) Nissl stain of section in the coronal plane with bilateral midline neocortical nodular heterotopia. Red box indicates area of enlargement in panel *D*. (*D*) Enlarged area from panel B. Arrows denote bilateral midline nodular heterotopia. (*E*) Section adjacent to panel *C* immunohistochemically stained for MBP. Red box indicates area of enlargement in panel *F*. (*F*) Enlarged area from panel *E*. Arrows denote bilateral midline nodular heterotopia. Bar in *E* for *C*,*E* = 1 mm. Bar in *F* for *D*,*F* = 500 μm. (*G*) Nissl stain of section in the horizontal plane with bilateral midline neocortical nodular heterotopia. Red box indicates area of enlargement in panel *H*. (*H*) Arrows denote bilateral midline nodular heterotopia. (*I*) Section adjacent to panel *G* immunohistochemically stained for MBP. Red box indicates area of enlargement in panel *J*. (*J*) Enlarged area from panel *I*. Arrows denote heterotopia. Bar in *I* for *G*,*I* = 1 mm. Bar in *J* for *H*,*J* = 500 μm. (*K*) Nissl stain of section in the sagittal plane with bilateral midline neocortical nodular heterotopia. Red box indicates area of enlargement in panel L. (*L*) Arrows denote bilateral midline nodular heterotopia. (*M*) Section adjacent to panel *K* immunohistochemically stained for MBP. Red box indicates area of enlargement in panel *M*. (*N*) Enlarged area from panel *M*. Arrows denote heterotopia. Bar in *M* for *K*,*M* = 1 mm. Bar in *N* for *L*,*N* = 500 μm.

Table 1
Volume measures (mean ± standard error of mean) in BXD29-*Tlr4*$^{lps2-J}$/J mutant and BXD29/Ty wildtype brains (cubic millimeter) and MSACC (square millimeters)

Region	BXD29-*Tlr4*$^{lps2-J}$/J	BXD29/Ty
Cerebral cortex	90.4 ± 1.5 (8)	85.4 ± 2.4 (8)
Cerebellum	48.3 ± 1.1 (8)	46.5 ± 0.9 (7)[a]
Hippocampus	24.5 ± 0.3 (8)	23.8 ± 0.6 (8)
Striatum	21.0 ± 0.7 (8)	20.3 ± 0.6 (8)
Total brain[b]	406.8 ± 6.2 (8)	370.4 ± 8.1 (7)[a]
Heterotopia[b]	1.9 ± 0.1 (8)	—(8)
MSACC[b]	0.514 ± 0.041 (8)	1.010 ± 0.044 (8)

[a]Cerebellum of one subject lost in histology.
[b]Indicates significant difference between mutant and wildtype, *N* in parentheses.

appear to dissipate until P10 (Fig. 4*F*). By P14, the heterotopias have taken on their adult-like appearance (Fig. 4*G*). BrdU birthdating demonstrates that the neurons in the heterotopia are generated midgestation to late gestation (Fig. 4*H–M*). There were few, if any, E12.5 BrdU+ cells and a relatively small number of densely labeled E14.5 BrdU+ cells were present in the lateral portions of the heterotopia (Fig. 4*J,K*). In contrast, there were large numbers of densely labeled E16.5 BrdU + neurons that were distributed throughout the heterotopia, although somewhat sparser in the lateral portions (Fig. 4*L,M*). These results confirm that neurons in the heterotopias are generated predominantly during midgestation-to late gestation.

There Are Disruptions of Callosal and Cingulum Fiber Tracts in the Mutant Mouse

We used HARDI tractography to assess fiber tract organization in BXD29-*Tlr4*$^{lps-2J}$/J mutant and BXD29/Ty wildtype mice. We performed a series of ANOVAs in each of the fiber tract measures (total brain, left and right intrahemispheric, corpus callosum, corticospinal, and left and right cingulum) with 4 dependent measures (number of tracts, length of tracts, FA, and ADC) and with strain as the independent measure. Preliminary repeated measures ANOVA revealed that there were no differences between left and right cingulum for any dependent measures, and so their results were pooled. A similar analysis for left and right intrahemispheric fibers revealed a significant difference in the number of tracts (left > right, $F_{1,6} = 9.9$, $P < 0.05$) and FA (left > right, $F_{1,6} = 6.5$, $P < 0.05$). We therefore pooled the intrahemispheric data for ADC ($F_{1,6} < 1$, not significant [NS]) and length ($F_{1,6} < 1$, NS) only.

Because the mutant strain has partial callosal agenesis, we anticipated that there would be fewer tracts passing through the callosum in this strain when compared with the wildtype, which turned out to be the case ($F_{1,6} = 11.8$, $P < 0.05$; Fig. 5*A,E,F*). There were also fewer cingulum fibers in the mutant strain as compared with the wildtype ($F_{1,6} = 10.9$, $P < 0.05$; Fig. 6*A*,G–I). There were no significant differences in tract number in the total brain ($F_{1,6} < 1$, NS), right or left intrahemispheric ($F_{1,6} < 1$, NS and $F_{1,6} = 1.8$, NS, respectively) or corticospinal measures ($F_{1,6} < 1$, NS). ADC was significantly decreased in mutant mice for total brain ($F_{1,6} = 11.9$, $P < 0.05$), intrahemispheric ($F_{1,6} = 32.2$ $P < 0.01$), callosum ($F_{1,6} = 6.9$, $P < 0.05$), corticospinal ($F_{1,6} = 9.6$, $P < 0.05$), and cingulum ($F_{1,6} = 37.5$, $P < 0.001$; Fig. 5*B*). In contrast, there were no differences between the strains in FA ($F_{1,6} < 1.3$, NS for all measures; Fig. 5*C*). The decrease in ADC without a concomitant change in FA suggests that there are fewer myelinated axons in the mutant mouse when compared with the wildtype. Mutant mice have shorter corticospinal ($F_{1,6} = 37.0$ $P < 0.001$) and cingulum tracts ($F_{1,6} = 16.5$, $P < 0.01$), but there are no differences in length of total brain, intrahemispheric, or callosal fibers ($F_{1,6} < 1.6$, NS for all measures; Fig. 5*D*).

Mutants Have a Selective and Severe Impairment in Rapid Auditory Processing

Auditory Testing

Initial tests revealed that both mutant and wildtype mice were able to detect single tones, indicating that both strains had comparable hearing and prepulse inhibition abilities ($t = 2.46$, degrees of freedom [df] = 7, $P < 0.05$; $t = 2.35$, df = 7, $P = 0.051$). The results from the normal single tone were used as a covariate for all further auditory processing tasks.

Silent gap 0–300 ms. A repeated measure ANOVA with Strain (mutant vs. wildtype) as the between measure and Day and Gap Duration as within measures revealed a main effect of Strain ($F_{1,13} = 35.7$, $P < 0.001$), indicating that wildtype mice were performing better than mutants. In addition to the main effect of Strain, a significant Strain × Gap Duration interaction ($F_{8,104} = 4.3$, $P < 0.001$) was found. This interaction reflected that the longer gaps (175–300 ms) were much easier for wildtype mice to perform in comparison to mutant mice, while the shorter gaps (50–150 ms) were more difficult for both groups of mice to perform (Fig. 6*A*). In order to confirm that the Treatment effect was not simply a reflection of failure by the mutants to detect the cue under any conditions, a paired samples *t*-test examining cued versus uncued startle responses was performed (within mutants) at the longest gap duration (300 ms). A significant difference ($t = 2.72$, df = 7; $P < 0.05$) reveals that mutants did show some discrimination at this easy condition.

Silent gap 0–100 ms. A repeated measure ANOVA with Strain (mutant vs. wildtype) as the between measure and Day and Gap Duration as within measures revealed a main effect of Strain ($F_{1,13} = 11.6$, $P < 0.01$), indicating that wildtype mice performed significantly better on the task than mutants. The ANOVA also revealed a significant Strain × Gap Duration interaction ($F_{8,104} = 7.3$, $P < 0.001$). This interaction showed that at the longer gaps (20–100 ms), wildtype mice were more effectively performing the task in comparison to mutant mice, however, performance at the shorter gaps (2–10 ms) showed that the task was more difficult for both groups (Fig. 6*A′*). Examination of cued versus uncued startle responses using a paired samples *t*-test showed a significant difference (within mutants) at the longest gap duration (100 ms) ($t = 3.42$, df = 7; $P < 0.05$) revealing that mutants did show some discrimination at this easy condition.

Motor Assessment: Rotarod

The results of the rotarod experiments are summarized in Figure 6*B*. A one-way ANOVA found no main effect of Strain ($F_{1,14} < 1$, NS), indicating that there was no overall difference in performance on the rotarod between the wildtype and mutant mice.

Water Maze Assessment: MWM

The results for the MWM are summarized in Figure 6*C*. A repeated measures ANOVA using Strain as the between

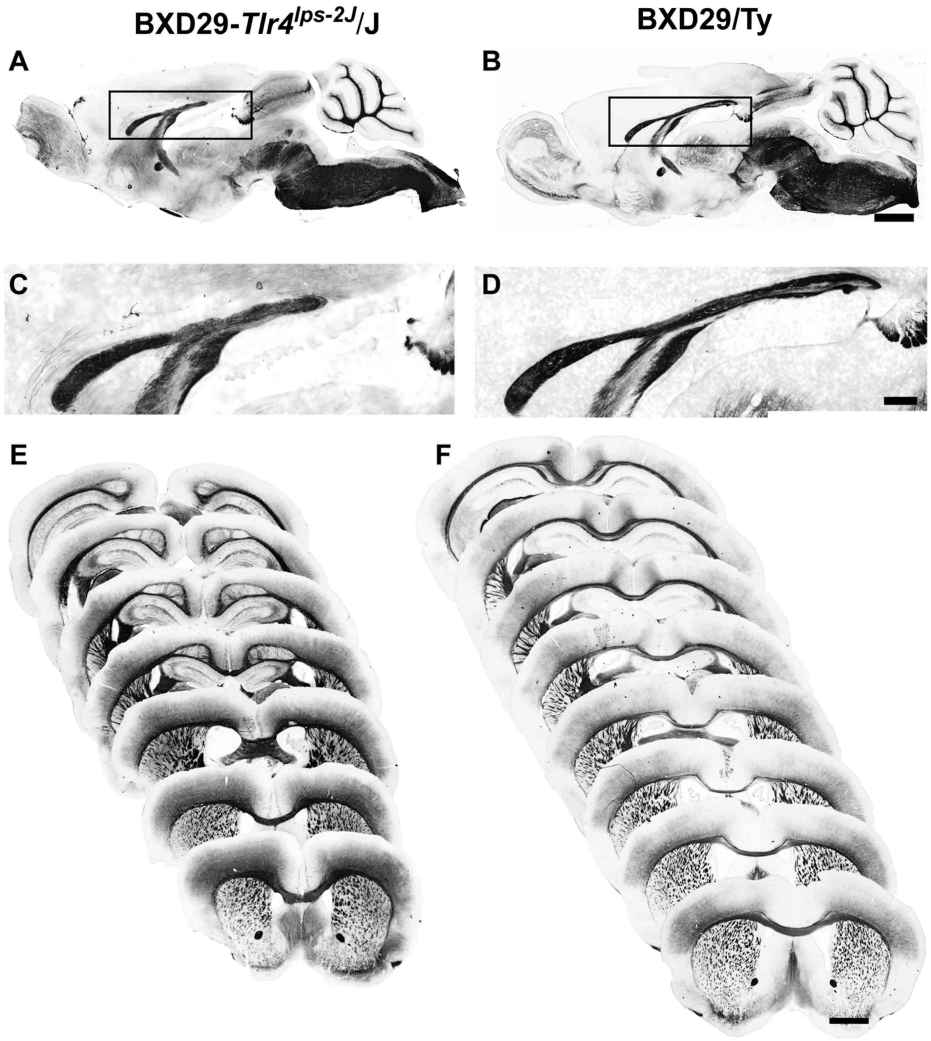

Figure 2. Photomontages of MBP-stained midsagittal sections from BXD29-*Tlr4*$^{lps\text{-}2J}$/J mutant (*A*) and BXD-29/Ty wildtype (*B*) mice illustrating partial agenesis of the corpus callosum. Boxes indicate area of enlargement in (*C*,*D*). Coronal sections from mutant (*E*) and wildtype (*F*) mice at 300 μm intervals indicating that agenesis of the caudal portion of the corpus callosum coincides with the onset of the malformation. Bars for *A*,*B*,*E*,*F* = 1 mm. Bar for *C*,*D* = 250 μm.

measure and Day as the within, revealed no main effect of Strain ($F_{1,14}$ < 1, NS), but did reveal a significant effect of Day ($F_{4,56}$ = 11.4, P < 0.001), which indicated that both wildtype and mutant groups improved in performance over time. Taken together, these results suggest that both groups learned the task equally well.

Water Maze Assessment: Nonspatial Water Maze

The results for the NSWM are summarized in Figure 6*D*. A repeated measures ANOVA using Strain as the between measure and Day as the within, revealed no main effect of Strain ($F_{1,14}$ < 1, NS), but as with the MWM, there was a significant effect of Day ($F_{4,56}$ = 3.6, P < 0.05), again suggesting that the performance on the task improved for both wildtype and mutant mice.

Genetics

Backcross Experiment

F1 progeny from a cross between mutant and wildtype animals were backcrossed to the mutants, producing 51 coisogenic N2 progeny segregating at *Tlr4* and any other new mutations. We screened both F1 parents and the backcross progeny for midline nodular heterotopias. None of the 8 F1s had any detectible malformations, demonstrating that the mutant phenotype is recessive. The penetrance of the mutation is 100% on the mutant background, and we therefore expected a 50% incidence of heterotopias in the backcross progeny. However, only 33% of progeny (17/51) had heterotopias, without difference in incidence by sex. If heterotopia was caused by the joint effects of both a single recessive allele and one or more modifier genes, then we would expect less than a 50% incidence. For example, if the heterotopia were fully penetrant but required a homozygous mutation in a second unlinked gene, then we could expect ~25% incidence in the backcross, close to the observed incidence. The current experiment is most consistent with a 2-hit autosomal recessive model of the neocortical mutation.

Evidence presented above indicates that no single gene, including the known *Tlr4* mutation, can be solely responsible for the heterotopia or partial agenesis of the corpus callosum. The result from the backcross suggests that at least 2 genes contribute to the mutant phenotype, and we therefore investigated whether the *Tlr4* mutation was acting as a modifier.

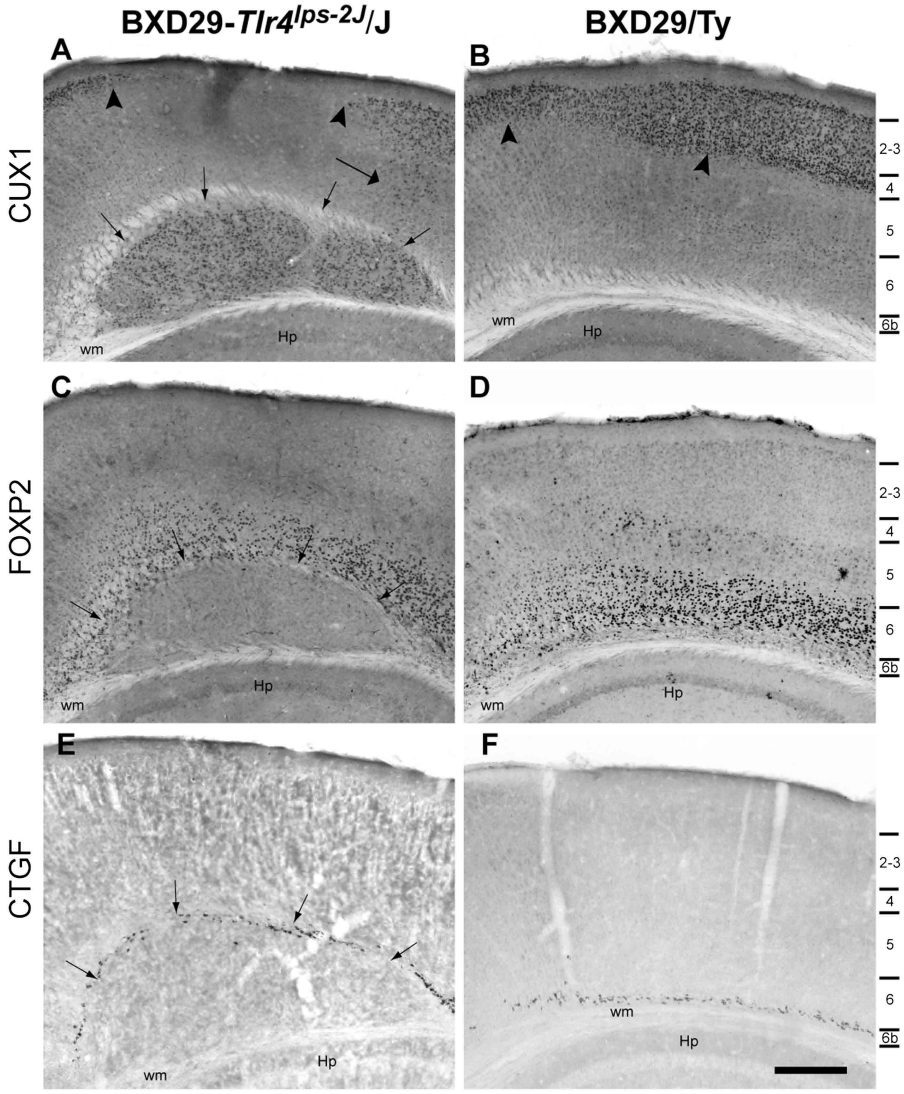

Figure 3. Laminar markers in BXD29-*Tlr4*$^{lps\text{-}2J}$/J mutant (*A*,*C*,*E*) and BXD29/Ty wildtype (*B*,*D*,*F*) mice. Photomicrograph of CUX1 immunoreactivity in heterotopia in mutant (*A*) and wildtype (*B*) mouse. Small arrows in panel *A* denote border of nodular heterotopia, which contains large numbers of CUX1 immunopositive neurons. Arrowheads in *A* highlight region of decreased density of CUX1 immunopositive neurons when compared to homologous region in WT neocortex in *B*. Large arrow denotes numbers of CUX1-positive neurons in lower cortical laminae, denoted on right side of figure. (*C*,*D*) Low power photomicrograph of section from mutant (*C*) and wildtype mice (*D*) immunohistochemically stained for FOXP2. There are immunopositive neurons superior to the border of the heterotopia. (*E*,*F*) Low power photomicrograph of CTGF immunoreactive neurons in mutant (*E*) and wildtype mice (*F*). CTGF neurons are located superior to the nodular heterotopia, and there are no CTGF neurons in the heterotopia itself (*E*). Hp = hippocampus, wm = white matter. Bar = 250 μm.

We genotyped the *Tlr4* gene of the backcross animals. Half of the progeny (n = 26) carried the mutant allele—a precise match to expectation. However, of the 17 progeny with heterotopias, only 11 carried the *Tlr4* mutation. These results make it highly unlikely that the *Tlr4* mutation contributes to the phenotype, even as a modifier.

Discussion

We have discovered a new mutation associated with bilateral midline subcortical nodular heterotopia and partial agenesis of the corpus callosum in the BXD29-*Tlr4*$^{lps\text{-}2J}$/J mouse strain. The mutation occurred and was fixed in this line between 1998 and 2004. We have been able to exclude the previously reported 8 bp insertion in the *Tlr4* gene (Cook et al. 2006) as causal. Immunohistochemical detection of laminar markers and BrdU studies confirm that the heterotopias in mutants are subcortical and are comprised of neurons generated in midgestation to late gestation that would mainly be destined for superficial layers of the neocortex. The segregation of the mutation in a test cross are consistent with a 2-locus autosomal recessive model. Partial callosal agenesis was confirmed by HARDI tractography, and there is evidence of disruption of cingulum fibers. Moreover, there is an overall decrease in ADC in the mutant mice as compared with the wildtype. Surprisingly, overall brain weight is 10% greater in mutants, suggesting pleiotropic effects that are not limited to neocortex. Behaviorally, mutant mice have a remarkable and selective defect in rapid auditory processing.

Disruptions of neocortical neuron migration result in wide variety neurologic abnormalities, including tuberous sclerosis, focal cortical dysplasia, hemimegalencephaly, classical lissencephaly, subcortical band heterotopia, periventricular nodular heterotopia, polymicrogyria, and schizencephaly. Malformations, in turn, are associated with a multiplicity of neurological outcomes ranging from profound mental retardation, epilepsy, and developmental dyslexia (Kuzniecky 2006; Guerrini et al.

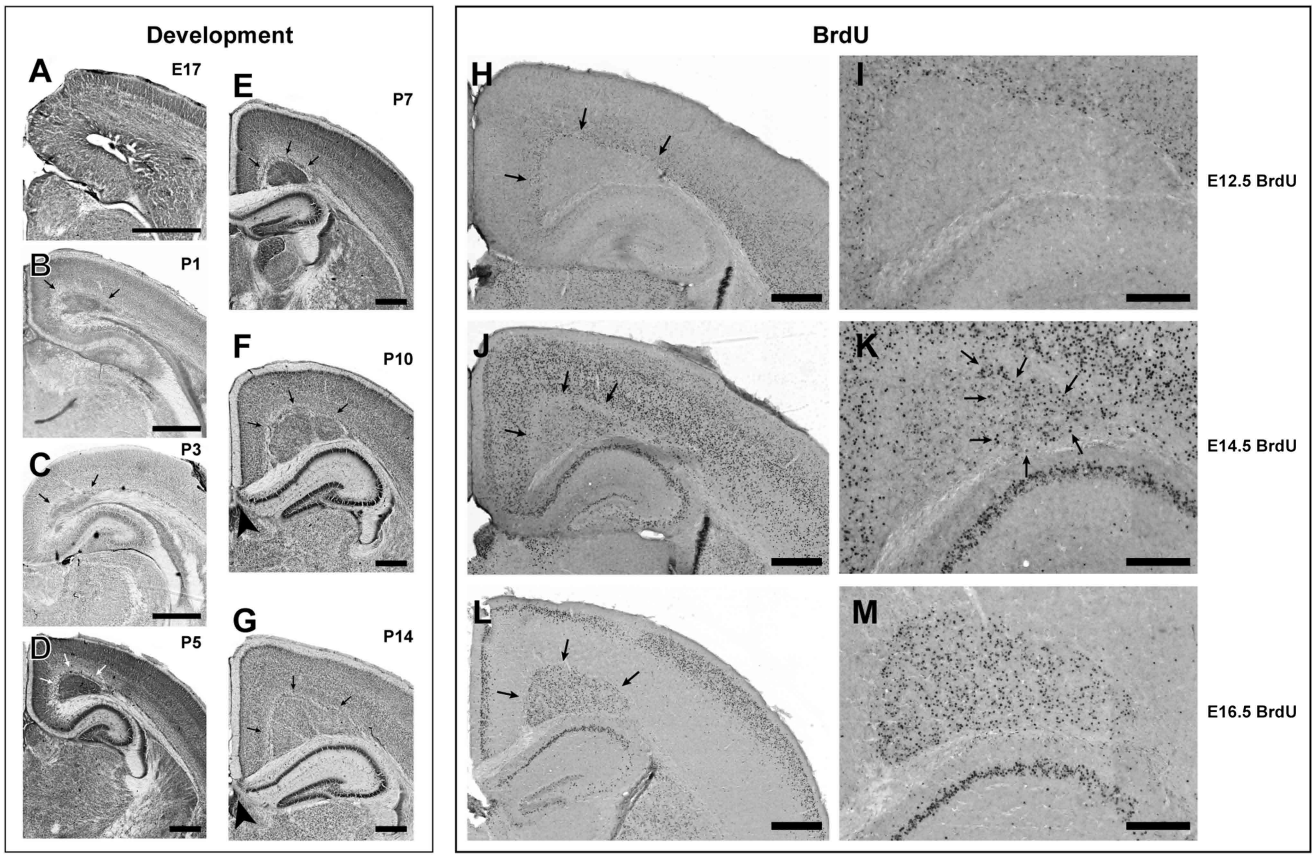

Figure 4. Development of bilateral subcortical midline heterotopias. Nissl-stained photomicrographs illustrating progression of heterotopia at E17 (*A*), P1 (*B*), P3 (*C*), P5 (*D*), P7 (*E*), P10 (*F*), and P14 (*G*). The first direct evidence of heterotopia formation appears at P1 (arrows in *B*). The density of neurons within the heterotopia decreases over time, as the volume of the heterotopia expands in concert with the expansion of the neocortex. Agenesis of the caudal portion of the corpus callosum can be seen in panels *F* and *G* (arrowheads). Panels *H*–*M* illustrate the results of BrdU experiments. (*H*) Low power micrograph illustrating the disposition of BrdU+ neurons in mutant mice following E12.5 injection. There are virtually no neurons in the heterotopia. (*I*) High power photomicrograph of panel *H* illustrating BrdU+ neurons in layer 6 directly dorsal to the heterotopia, but no neurons within. (*J*) Low power micrograph illustrating the disposition of BrdU+ neurons in mutant mice following E14.5 injection. There are relatively few densely labeled BrdU + neurons in the lateral-most regions of the heterotopia. (*K*) High power photomicrograph of panel *J* illustrating clusters of BrdU+ neurons in the lateral-most portion of the heterotopia (arrows). (*L*) Low power photomicrograph illustrating the disposition of BrdU+ neurons in mutant mice following E16.5 injection. There are large numbers of densely labeled BrdU+ neurons in the heterotopia and in layers 2–3 of the neocortex. (*M*) High power photomicrograph of panel *L* illustrating clusters of BrdU+ neurons throughout the heterotopia but with a somewhat sparser distribution in the lateral portion of the heterotopia.

2008; Andrade 2009). The malformations reported here share characteristics with subcortical band heterotopia and periventricular nodular heterotopias, but do not entirely fit either classification. Similar to the former, the heterotopias in the mutant are located subcortically and in that respect resemble the location of subcortical band heterotopia. The nodular appearance is similar to that seen in periventricular nodular heterotopia, although the general location is different (Bai et al. 2003; Andrade 2009; Ferland et al. 2009; Spalice et al. 2009; Verrotti et al. 2010).

Croquelois et al. (2009) recently described a mouse mutant (HeCo) that has a heterotopia similar to BXD29. The heterotopia is located in a similar location (although slightly more lateral) and is described as containing heterotopic cortex that is separated by white matter from the homotopic cortex. This malformation is due to an autosomal recessive mutation, presumably from a single, as yet unidentified, gene. As with the BXD29 mutant, most of the neurons in both malformations are generated late in gestation. Croquelois and colleagues do not report partial callosal agenesis in the HeCo mouse, and their Figure 1 suggests that the callosum is unaffected. They classify their heterotopia as a subcortical band heterotopia based on its developmental similarity to the *Dcx* mutations. Despite some similarities, these differences suggest that BXD29 and the HeCo mutant are caused by different mutations, a prediction that should be tested by complementation.

The majority of neurons in the heterotopia in the BXD29 mutant are generated in midgestation to late gestation and are destined for layers 2–4 of the cerebral cortex. Nodular heterotopias in humans (Garbelli et al. 2009) and BCNU-treated rats (Moroni et al. 2009) have been reported to have rudimentary laminar organization. There is little evidence of laminar organization in the BXD29 mutant heterotopias. Neurons generated at E16.5 are found scattered throughout the malformation, and the majority of neurons in the heterotopia are CUX1 positive. On the other hand, neurons generated at E14.5 are concentrated toward at the lateral edges of the heterotopia, indicative of at least some regional differentiation.

In addition to the heterotopias in the BXD29 mutant, all mice had partial callosal agenesis. A large percentage of fetuses with callosal agenesis identified by sonography have heterotopias and other neuronal migration disorders (Volpe et al. 2006). In addition, there are syndromes in humans where callosal agenesis is accompanied by neuronal migration disorders. Aicardi

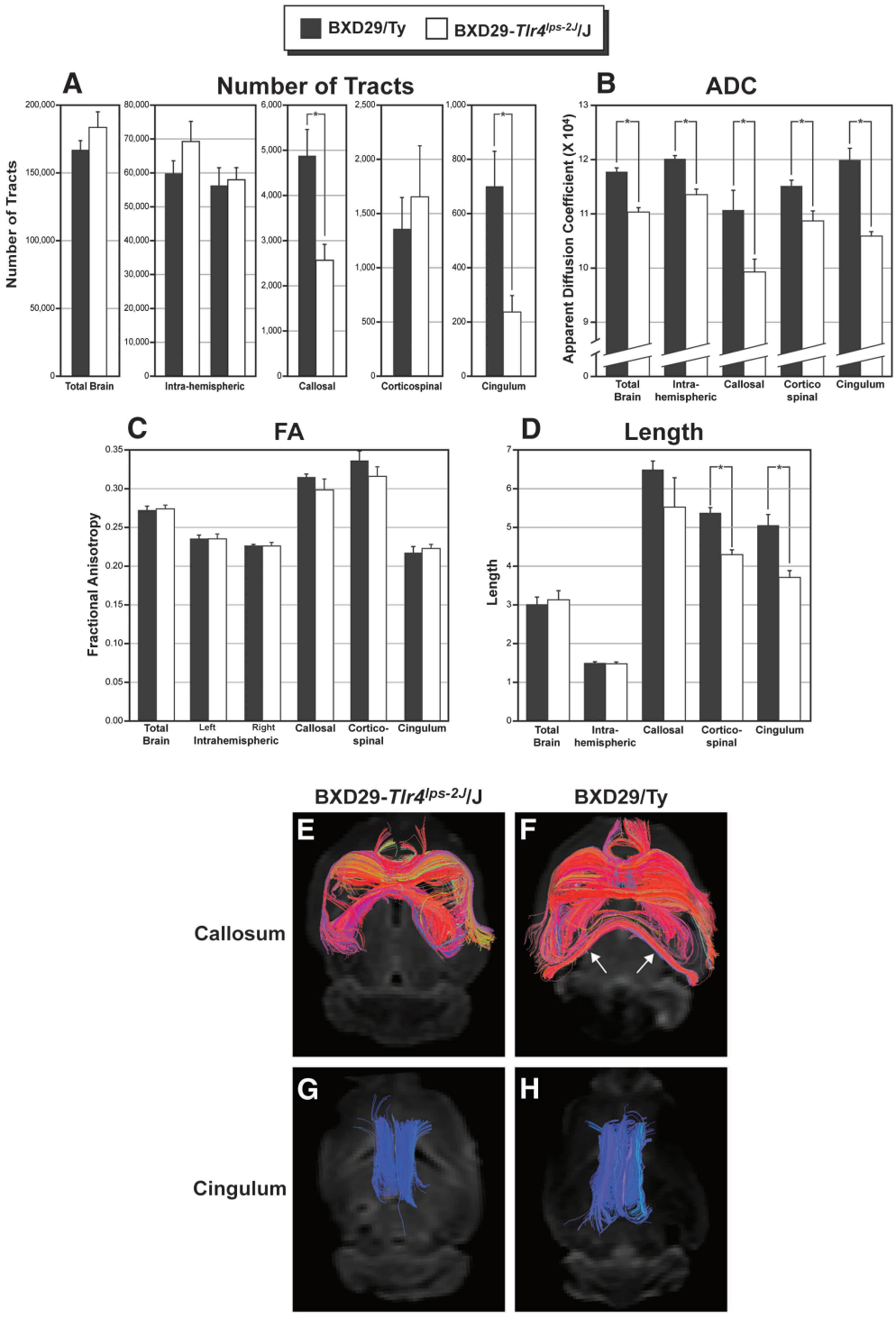

Figure 5. High angular resolution diffusion imaging (HARDI) tractography of the brains of BXD29-*Tlr4*$^{lps\text{-}2J}$/J mutant and BXD29/Ty wildtype mice. Quantitative results of tract number (*A*), ADC (*B*), FA (*C*), and length (*D*) from total brain, intrahemispheric (right and left), callosal, corticospinal, and cingulum of wildtype (black bars) and mutant (white bars). (*A*) There is a significant decrease in the number of tractography pathways passing through the corpus callosum of mutant mice when compared to the wildtype. In addition, there is a decrease in the number of cingulum tractography pathways in the mutant mice. There were no significant differences in the number of tracts in any of the other tractography pathways. (*B*) There is a significant decrease in ADC in mutant compared with wildtype mice across all tract categories. (*C*) There is no significant difference in FA among the tract categories. (*D*) The length of corticospinal tracts and cingulum are decreased in the mutant as compared to wildtype. There are no significant differences in the length of fiber tracts in any of the other tract measures. (*E*,*F*) Visualization of tractography pathways passing through the corpus callosum of mutant (*E*) and wildtype (*F*) mice. There are fewer callosal tracts in the mutant as compared to the wildtype, and there is a lack of interhemispheric tracts in the caudal regions of the forebrain (arrows). (*G*,*H*). Visualization of cingulum fiber tracts in the left and right hemispheres of mutant (*G*) and wildtype (*H*) mice. There are fewer and shorter fibers in the mutant cingulum as compared to the wildtype.

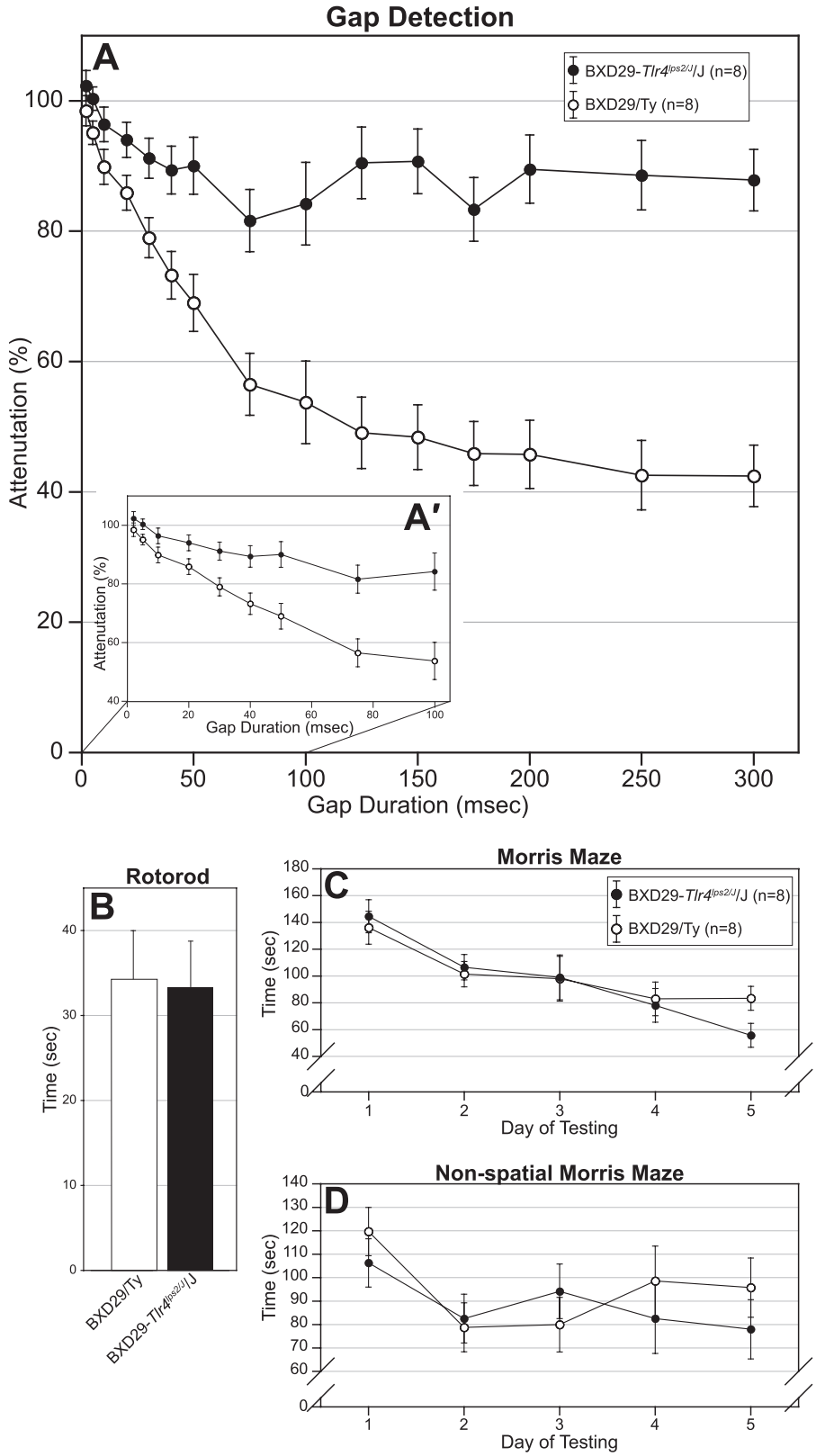

Figure 6. Behavioral tests of BXD29-*Tlr4*$^{lps\text{-}2J}$ /J mutant and BXD29/Ty wildtype strain. (*A*) SG 0–300 ms and SG 0–100 ms data are combined; see (*A′*) for SG 0–100 ms data only. Mutant mice are significantly impaired in rapid auditory processing as assessed by startle reduction in a gap detection task. There is no difference (and no attenuation between mutant and wildtype mice at the shortest gap durations [50–150 ms and 2–10 ms] for the SG 0–300 and SG 0–100 ms task, respectively see *A* and *A′*, respectively), but the mutant significantly attenuates at the 300 ms gap durations for the SG 0–300 ms task and at the 100 ms gap for the SG 0–100 ms task. There are no differences between the strains on rotarod (*B*), Morris maze (*C*), or nonspatial Morris maze (*D*).

syndrome is associated with periventricular nodular heterotopias as well as callosal agenesis (Smith et al. 1996; Hopkins et al. 2008). Callosal agenesis (Zamponi et al. 2002) and migrational disturbances (Şenocak et al. 2010) have been reported in Joubert syndrome, a genetic disorder generally affecting the brain stem and cerebellum. In mice, callosal agenesis has been reported in *Dcx* knockout mice on a 129/SvPas genetic background (Kappeler et al. 2007) but not on a C57BL/6N background. Unlike humans with *DCX* mutations, these mice do not have cortical migration anomalies, but do exhibit migration disturbances in the hippocampus. Furthermore, these authors report callosal agenesis of varying severity in humans with *DCX* type I lissencephaly, with agyria.

HARDI tractography indicated a decrease of callosal fiber tracts in the BXD29 mutant, as well as decrease in the number of cingulum fiber tracts. These results were predicted based on both the partial callosal agenesis and the location of heterotopias, which should disrupt cingulum fibers. Because HARDI only measures coherence of fiber tracts, however, we cannot exclude the possibility that the cingulum fiber tracts are of equal length between the 2 strains, but deviate around the heterotopias. In addition to the changes in fiber tract length, there was a decrease in ADC in all fiber tracts in the mutant. We have previously reported that ADC variation is dependent on the degree of myelination (Takahashi et al. 2011). Thus, immature brains with minimal myelin can have significantly lower ADC values than fully myelinated brains after fixation, possibly due to the larger extracellular space available (Takahashi et al. 2011).

Although neuronal migration disorders are not always associated with changes in connectivity (Caviness and Yorke 1976; Caviness and Frost 1983; Schottler et al. 1998), there is prior evidence linking widespread changes in neuronal connections to developmental malformations. Jenner et al. (2000) found distinct bundles of fibers extending from neurons in molecular layer heterotopias in NZB/BlNJ mice, and that some fibers traversed the corpus callosum and others the internal capsule. A number of investigators have demonstrated both homotopic and heterotopic corticocortical projections, as well as aberrant thalamocortical projections associated with an animal model of polymicrogyria induced by perinatal freeze lesions (Giannetti et al. 1999, 2000; Rosen et al. 2000). Similar abnormalities in connectivity in humans are now beginning to be reported. For example, in partial agenesis of the corpus callosum, increased heterotopic connections have also been identified (Wahl et al. 2009).

BXD29-*Tlr4*$^{lps\text{-}2J}$/J mutants have a severe defect in rapid auditory processing, despite normal hearing. Gap detection results showed that while normal BXD mice could detect silent gaps of 5 ms or greater, mutant BXD subjects did not reach criterion for discrimination until 20 ms. Moreover, the plateau in performance for BXD mutants between 100 and 300 ms stimuli suggests that even at these longer gap durations, the mutants remain substantially worse than controls. Importantly, comparable results between the 2 groups on the single-tone task reinforce the view that baseline hearing or PPI deficits in the mutants cannot account for this effect. The acoustic processing deficit instead appears to reflect a profound difficulty with acoustic stimuli that are more complex than a single tone and still relatively "short" (up to 300 ms) in duration. Previous research has demonstrated a strong link between defects in rapid auditory processing and neuronal migration disorders. Rats with migration disorders either induced by freeze lesions on P1 (Fitch et al. 1994; Clark et al. 2000; Peiffer et al. 2004), by embryonic knockdown of neuronal migration genes (Threlkeld et al. 2007), or by prenatal exposure to methylazoxymethanol (Threlkeld et al. 2009) have auditory processing deficits similar to those reported here. Mice with spontaneously occurring molecular layer ectopias are similarly affected (Peiffer et al. 2001, 2002), and this processing defect is reflected by electrophysiologic measures (Frenkel et al. 2000). Our results are therefore compatible with the notion that neuronal migration disorders are associated with defects in sensory processing. Interestingly, mutant mice did not differ from coisogenic wildtype mice on motor and spatial and nonspatial memory tasks—both groups performed the task to criteria equally well. This suggests that the neuronal migration anomalies associated with the BXD29-*Tlr4*$^{lps\text{-}2J}$/J mutant mouse disrupted specific sensory domains related to rapid auditory processing and thus not indicative of a global reorganization of several neural systems.

The appearance of bilateral subcortical nodular heterotopias and partial callosal agenesis in the BXD29-*Tlr4*$^{lps\text{-}2J}$/J mutant mouse coincided roughly with the report of *Tlr4*-mediated LPS insensitivity in this strain (Cook et al. 2004, 2006). This raised the possibility that the *Tlr4* mutation was itself causal. However, we have shown that other strains with spontaneous mutations in this gene (C57BL/10ScNJ and B6.B10ScN-*Tlr4*$^{lps\text{-}del}$/J) do not have cortical malformations nor do knockouts of other genes in the TLR4 pathway (B6.129-*Tlr2*^{tm1Kir}/J and Myd88$^{-/-}$). Results from the coisogenic backcross experiment are most consistent with the hypothesis that the mutant phenotype is controlled by 2 independent genes, and that *Tlr4* is not involved even as a modifier. The BXD29-*Tlr4*$^{lps\text{-}2J}$/J mutant appears to have fixed at least 3 spontaneous mutations over a relatively short period of 30 years. Recent sequencing of human families has shown that single individuals harbor 30–50 spontaneous mutations (Conrad et al. 2011). Given this single generation mutation rate, it is certainly plausible that 2 mutations modulating cortical development could have been fixed in the genome of BXD29 over a period of 30 years or ~100 generations of full sib matings.

The invariant location of the bilateral heterotopia—at the boundary between dorsal parietal/visual neocortex on the lateral side and retrosplenial cortex on the medial side—provides an important clue as to the types of genes likely to be mutated. We predict that the mutation will target genes with a key role patterning and/or migration of neurons in this relatively restricted zone. Analysis of images in the Allen Brain Institute's atlas of gene expression in the mouse brain reveals a number of genes whose expression respects this architectonic border, some of which are included in Supplementary Figure 1. Future experiments aimed at elucidating sequence differences between mutant and wildtype will directly address this issue.

Supplementary Material

Supplementary material can be found at: http://www.cercor.oxfordjournals.org/

Funding

The National Institute on Drug Abuse and the National Institute of Mental Health (grant number P20 DA021131); the National Institute of Neurological Diseases and Stroke (grant number

R01 NS052397-01A2); the National Eye Institute (grant number R01EY021200), and Shared Instrumentation Grants from the National Center for Research Resources (grant numbers 1S10RR023401, 1S10RR019307, and 1S10RR023043), which are all at the National Institutes of Health.

Notes

We thank G. Allan Johnson and the Center for In Vivo Microscopy for providing MRI images used in Figure 1. We also thank Jacob Sloane for providing Tlr2–/– and Myd88–/– mice. *Conflict of Interest:* None declared.

References

Andrade DM. 2009. Genetic basis in epilepsies caused by malformations of cortical development and in those with structurally normal brain. Hum Genet. 126:173–193.

Bai J, Ramos RL, Ackman JB, Thomas AM, Lee RV, LoTurco JJ. 2003. RNAi reveals doublecortin is required for radial migration in rat neocortex. Nat Neurosci. 6:1277–1283.

Bilasy SE, Satoh T, Ueda S, Wei P, Kanemura H, Aiba A, Terashima T, Kataoka T. 2009. Dorsal telencephalon-specific RA-GEF-1 knockout mice develop heterotopic cortical mass and commissural fiber defect. Eur J Neurosci. 29:1994–2008.

Caviness VS Jr, Frost DO. 1983. Thalamocortical projections in the reeler mutant mouse. J Comp Neurol. 219:182–202.

Caviness VS Jr, So DK, Sidman RL. 1972. The hybrid reeler mouse. J Hered. 63:241–246.

Caviness VS Jr, Yorke CH Jr. 1976. Interhemispheric neocortical connections of the corpus callosum in the reeler mutant mouse: a study based on anterograde and retrograde methods. J Comp Neurol. 170:449–460.

Chang BS, Piao X, Giannini C, Cascino GD, Scheffer I, Woods CG, Topcu M, Tezcan K, Bodell A, Leventer RJ, et al. 2004. Bilateral generalized polymicrogyria (BGP): a distinct syndrome of cortical malformation. Neurology. 62:1722–1728.

Chen ZF, Schottler F, Bertram E, Gall CM, Anzivino MJ, Lee KS. 2000. Distribution and initiation of seizure activity in a rat brain with subcortical band heterotopia. Epilepsia. 41:493–501.

Clark MG, Rosen GD, Tallal P, Fitch RH. 2000. Impaired processing of complex auditory stimuli in rats with induced cerebrocortical microgyria: an animal model of developmental language disabilities. J Cogn Neurosci. 12:828–839.

Conrad DF, Keebler JE, DePristo MA, Lindsay SJ, Zhang Y, Casals F, Idaghdour Y, Hartl CL, Torroja C, Garimella KV, et al. 2011. Variation in genome-wide mutation rates within and between human families. Nat Genet. 43:712–714.

Cook DN, Wang S, Wang Y, Howles GP, Whitehead GS, Berman KG, Church TD, Frank BC, Gaspard RM, Yu Y, et al. 2004. Genetic regulation of endotoxin-induced airway disease. Genomics. 83: 961–969.

Cook DN, Whitehead GS, Burch LH, Berman KG, Kapadia Z, Wohlford-Lenane C, Schwartz DA. 2006. Spontaneous mutations in recombinant inbred mice: mutant toll-like receptor 4 (Tlr4) in BXD29 mice. Genetics. 172:1751–1755.

Croquelois A, Giuliani F, Savary C, Kielar M, Amiot C, Schenk F, Welker E. 2009. Characterization of the HeCo mutant mouse: a new model of subcortical band heterotopia associated with seizures and behavioral deficits. Cereb Cortex. 19:563–575.

des Portes V, Pinard JM, Billuart P, Vinet MC, Koulakoff A, Carrie A, Gelot A, Dupuis E, Motte J, Berwald-Netter Y, et al. 1998. A novel CNS gene required for neuronal migration and involved in X- linked subcortical laminar heterotopia and lissencephaly syndrome. Cell. 92:51–61.

Dobyns WB, Andermann E, Andermann F, Czapansky-Beilman D, Dubeau F, Dulac O, Guerrini R, Hirsch B, Ledbetter DH, Lee NS, et al. 1996. X-linked malformations of neuronal migration. Neurology. 47:331–339.

Dobyns WB, Guerrini R, Czapansky-Beilman DK, Pierpont ME, Breningstall G, Yock DH Jr, Bonanni P, Truwit CL. 1997. Bilateral periventricular nodular heterotopia with mental retardation and syndactyly in boys: a new X-linked mental retardation syndrome. Neurology. 49:1042–1047.

Ferland RJ, Batiz LF, Neal J, Lian G, Bundock E, Lu J, Hsiao YC, Diamond R, Mei D, Banham AH, et al. 2009. Disruption of neural progenitors along the ventricular and subventricular zones in periventricular heterotopia. Hum Mol Genet. 18:497–516.

Ferland RJ, Cherry TJ, Preware PO, Morrisey EE, Walsh CA. 2003. Characterization of Foxp2 and Foxp1 mRNA and protein in the developing and mature brain. J Comp Neurol. 460:266–279.

Fitch RH, Tallal P, Brown C, Galaburda AM, Rosen GD. 1994. Induced microgyria and auditory temporal processing in rats: a model for language impairment? Cereb Cortex. 4:260–270.

Fitch RH, Threlkeld SW, McClure MM, Peiffer AM. 2008. Use of a modified prepulse inhibition paradigm to assess complex auditory discrimination in rodents. Brain Res Bull. 76:1–7.

Frenkel M, Sherman GF, Bashan KA, Galaburda AM, LoTurco JJ. 2000. Neocortical ectopias are associated with attenuated neurophysiological responses to rapidly changing auditory stimuli. Neuroreport. 11:575–579.

Garbelli R, Rossini L, Moroni RF, Watakabe A, Yamamori T, Tassi L, Bramerio M, Russo GL, Frassoni C, Spreafico R. 2009. Layer-specific genes reveal a rudimentary laminar pattern in human nodular heterotopia. Neurology. 73:746–753.

Giannetti S, Gaglini P, Di Rocco F, Di Rocco C, Granato A. 2000. Organization of cortico-cortical associative projections in a rat model of microgyria. Neuroreport. 11:2185–2189.

Giannetti S, Gaglini P, Granato A, Di Rocco C. 1999. Organization of callosal connections in rats with experimentally induced microgyria. Childs Nerv Syst. 15:444–448; discussion 449–450.

Gleeson JG. 2000. Classical lissencephaly and double cortex (subcortical band heterotopia): lIS1 and doublecortin. Curr Opin Neurol. 13:121–125.

Gleeson JG, Allen KM, Fox JW, Lamperti ED, Berkovic S, Scheffer I, Cooper EC, Dobyns WB, Minnerath SR, Ross ME, et al. 1998. Doublecortin, a brain-specific gene mutated in human X-linked lissencephaly and double cortex syndrome, encodes a putative signaling protein. Cell. 92:63–72.

Goryunov D, He CZ, Lin CS, Leung CL, Liem RK. 2010. Nervous-tissue-specific elimination of microtubule-actin crosslinking factor 1a results in multiple developmental defects in the mouse brain. Mol Cell Neurosci. 44:1–14.

Guerrini R, Dobyns WB, Barkovich AJ. 2008. Abnormal development of the human cerebral cortex: genetics, functional consequences and treatment options. Trends Neurosci. 31: 154–162.

Guerrini R, Filippi T. 2005. Neuronal migration disorders, genetics, and epileptogenesis. J Child Neurol. 20:287–299.

Gundersen HJG, Jensen EB. 1987. The efficiency of systematic sampling in stereology and its prediction. J Microsc. 147:229–263.

Heuer H, Christ S, Friedrichsen S, Brauer D, Winckler M, Bauer K, Raivich G. 2003. Connective tissue growth factor: a novel marker of layer VII neurons in the rat cerebral cortex. Neuroscience. 119:43–52.

Hisaoka T, Nakamura Y, Senba E, Morikawa Y. 2010. The forkhead transcription factors, Foxp1 and Foxp2, identify different subpopulations of projection neurons in the mouse cerebral cortex. Neuroscience. 166:551–563.

Hopkins B, Sutton VR, Lewis RA, Van den Veyver I, Clark G. 2008. Neuroimaging aspects of Aicardi syndrome. Am J Med Genet A. 146A:2871–2878.

Jansen A, Andermann E. 2005. Genetics of the polymicrogyria syndromes. J Med Genet. 42:369–378.

Jenner AR, Galaburda AM, Sherman GF. 2000. Connectivity of ectopic neurons in the molecular layer of the somatosensory cortex in autoimmune mice. Cereb Cortex. 10:1005–1013.

Kappeler C, Dhenain M, Phan Dinh Tuy F, Saillour Y, Marty S, Fallet-Bianco C, Souville I, Souil E, Pinard JM, Meyer G, et al. 2007. Magnetic resonance imaging and histological studies of corpus callosal and hippocampal abnormalities linked to doublecortin deficiency. J Comp Neurol. 500:239–254.

Keays DA, Tian G, Poirier K, Huang GJ, Siebold C, Cleak J, Oliver PL, Fray M, Harvey RJ, Molnar Z, et al. 2007. Mutations in alpha-tubulin cause abnormal neuronal migration in mice and lissencephaly in humans. Cell. 128:45–57.

Kuzniecky RI. 2006. Malformations of cortical development and epilepsy, part 1: diagnosis and classification scheme. Rev Neurol Dis. 3:151–162.

Lammens M. 2000. Neuronal migration disorders in man. Eur J Morphol. 38:327–333.

Lee KS, Schottler F, Collins JL, Lanzino G, Couture D, Rao A, Hiramatsu K, Goto Y, Hong SC, Caner H, et al. 1997. A genetic animal model of human neocortical heterotopia associated with seizures. J Neurosci. 17:6236–6242.

Lein ES, Hawrylycz MJ, Ao N, Ayres M, Bensinger A, Bernard A, Boe AF, Boguski MS, Brockway KS, Byrnes EJ, et al. 2007. Genome-wide atlas of gene expression in the adult mouse brain. Nature. 445: 168–176.

Leventer RJ, Guerrini R, Dobyns WB. 2008. Malformations of cortical development and epilepsy. Dialogues Clin Neurosci. 10:47–62.

Leventer RJ, Mills PL, Dobyns WB. 2000. X-linked malformations of cortical development. Am J Med Genet. 97:213–220.

Mori S, Crain BJ, Chacko VP, van Zijl PC. 1999. Three-dimensional tracking of axonal projections in the brain by magnetic resonance imaging. Ann Neurol. 45:265–269.

Moroni RF, Inverardi F, Regondi MC, Watakabe A, Yamamori T, Spreafico R, Frassoni C. 2009. Expression of layer-specific markers in the adult neocortex of BCNU-Treated rat, a model of cortical dysplasia. Neuroscience. 159:682–691.

Ng L, Bernard A, Lau C, Overly CC, Dong HW, Kuan C, Pathak S, Sunkin SM, Dang C, Bohland JW, et al. 2009. An anatomic gene expression atlas of the adult mouse brain. Nat Neurosci. 12:356–362.

Nieto M, Monuki ES, Tang H, Imitola J, Haubst N, Khoury SJ, Cunningham J, Gotz M, Walsh CA. 2004. Expression of Cux-1 and Cux-2 in the subventricular zone and upper layers II-IV of the cerebral cortex. J Comp Neurol. 479:168–180.

Peiffer AM, Dunleavy CK, Frenkel M, Gabel LA, LoTurco JJ, Rosen GD, Fitch RH. 2001. Impaired detection of variable duration embedded tones in ectopic NZB/BINJ mice. Neuroreport. 12:2875–2879.

Peiffer AM, McClure MM, Threlkeld SW, Rosen GD, Fitch RH. 2004. Severity of focal microgyria and associated rapid auditory processing deficits. Neuroreport. 15:1923–1926.

Peiffer AM, Rosen GD, Fitch RH. 2002. Sex differences in rapid auditory processing deficits in ectopic BXSB/MpJ mice. Neuroreport. 13: 2277–2280.

Pilz DT, Matsumoto N, Minnerath S, Mills P, Gleeson JG, Allen KM, Walsh CA, Barkovich AJ, Dobyns WB, Ledbetter DH, et al. 1998. LIS1 and XLIS (DCX) mutations cause most classical lissencephaly, but different patterns of malformation. Hum Mol Genet. 7: 2029–2037.

Ramos RL, Smith PT, DeCola C, Tam D, Corzo O, Brumberg JC. 2008. Cytoarchitecture and transcriptional profiles of neocortical malformations in inbred mice. Cereb Cortex. 18:2614–2628.

Rosen GD, Burstein D, Galaburda AM. 2000. Changes in efferent and afferent connectivity in rats with cerebrocortical microgyria. J Comp Neurol. 418:423–440.

Rosen GD, Harry JD. 1990. Brain volume estimation from serial section measurements: a comparison of methodologies. J Neurosci Meth. 35:115–124.

Schmahmann JD, Pandya DN, Wang R, Dai G, D'Arceuil HE, de Crespigny AJ, Wedeen VJ. 2007. Association fibre pathways of the brain: parallel observations from diffusion spectrum imaging and autoradiography. Brain. 130:630–653.

Schottler F, Couture D, Rao A, Kahn H, Lee KS. 1998. Subcortical connections of normotopic and heterotopic neurons in sensory and motor cortices of the tish mutant rat. J Comp Neurol. 395: 29–42.

Şenocak EU, Oğuz KK, Haliloğlu G, Topçu M, Cila A. 2010. Structural abnormalities of the brain other than molar tooth sign in Joubert syndrome-related disorders. Diagn Interv Radiol. 16:3–6.

Sherman GF, Galaburda AM, Behan PO, Rosen GD. 1987. Neuroanatomical anomalies in autoimmune mice. Acta Neuropathol (Berlin). 74:239–242.

Sherman GF, Morrison L, Rosen GD, Behan PO, Galaburda AM. 1990. Brain abnormalities in immune defective mice. Brain Res. 532:25–33.

Smith CD, Ryan SJ, Hoover SL, Baumann RJ. 1996. Magnetic resonance imaging of the brain in Aicardi's syndrome. Report of 20 patients. J Neuroimaging. 6:214–221.

Soumiya H, Fukumitsu H, Furukawa S. 2009. Stem cell factor induces heterotopic accumulation of cells (heterotopia) in the mouse cerebral cortex. Biomed Res. 30:121–128.

Spalice A, Parisi P, Nicita F, Pizzardi G, Del Balzo F, Iannetti P. 2009. Neuronal migration disorders: clinical, neuroradiologic and genetics aspects. Acta Paediatr. 98:421–433.

Takahashi E, Dai G, Rosen GD, Wang R, Ohki K, Folkerth RD, Galaburda AM, Wedeen VJ, Grant PE. 2011. Developing neocortex organization and connectivity in cats revealed by direct correlation of diffusion tractography and histology. Cereb Cortex. 21:200–211.

Takahashi E, Dai G, Wang R, Ohki K, Rosen GD, Galaburda AM, Grant PE, Wedeen VJ. 2010. Development of cerebral fiber pathways in cats revealed by diffusion spectrum imaging. Neuroimage. 49:1231–1240.

Threlkeld SW, Hill CA, Cleary CE, Trong DT, Rosen GD, Fitch RH. 2009. Developmental learning impairments in a rodent model of nodular heterotopia. J Neurodev Disord. 1:237–250.

Threlkeld SW, McClure MM, Bai J, Wang Y, LoTurco JJ, Rosen GD, Fitch RH. 2007. Developmental disruptions and behavioral impairments in rats following in utero RNAi of Dyx1c1. Brain Res Bull. 71:508–514.

Trotter SA, Kapur J, Anzivino MJ, Lee KS. 2006. GABAergic Synaptic inhibition is reduced before seizure onset in a genetic model of cortical malformation. J Neurosci. 26:10756–10767.

Truett GE, Heeger P, Mynatt RL, Truett AA, Walker JA, Warman ML. 2000. Preparation of PCR-quality mouse genomic DNA with hot sodium hydroxide and tris (HotSHOT). Biotechniques. 29:52–54.

Verrotti A, Spalice A, Ursitti F, Papetti L, Mariani R, Castronovo A, Mastrangelo M, Iannetti P. 2010. New trends in neuronal migration disorders. Eur J Paediatr Neurol. 14:1–12.

Vishwas MS, Chitnis T, Pienaar R, Healy BC, Grant PE. 2010. Tract-based analysis of callosal, projection, and association pathways in pediatric patients with multiple sclerosis: a preliminary study. AJNR Am J Neuroradiol. 31:121–128.

Volpe P, Paladini D, Resta M, Stanziano A, Salvatore M, Quarantelli M, De Robertis V, Buonadonna AL, Caruso G, Gentile M. 2006. Characteristics, associations and outcome of partial agenesis of the corpus callosum in the fetus. Ultrasound Obstet Gynecol. 27:509–516.

Wahl M, Strominger Z, Jeremy RJ, Barkovich AJ, Wakahiro M, Sherr EH, Mukherjee P. 2009. Variability of homotopic and heterotopic callosal connectivity in partial agenesis of the corpus callosum: a 3T diffusion tensor imaging and Q-ball tractography study. AJNR Am J Neuroradiol. 30:282–289.

Wedeen VJ, Wang RP, Schmahmann JD, Benner T, Tseng WY, Dai G, Pandya DN, Hagmann P, D'Arceuil H, de Crespigny AJ. 2008. Diffusion spectrum magnetic resonance imaging (DSI) tractography of crossing fibers. Neuroimage. 41:1267–1277.

Zamponi N, Rossi B, Messori A, Polonara G, Regnicolo L, Cardinali C. 2002. Joubert syndrome with associated corpus callosum agenesis. Eur J Paediatr Neurol. 6:63–66.